Parametric generation and characterization of femtosecond mid-infrared pulses in $ZnGeP_2$

Scott Wandel,[1] Ming-Wei Lin,[1] Yanchun Yin,[1] Guibao Xu,[1] and Igor Jovanovic[1,2,*]

[1]*Department of Mechanical and Nuclear Engineering, The Pennsylvania State University, University Park, PA 16802, USA*

[2]*Department of Nuclear Engineering and Radiological Sciences, University of Michigan, Ann Arbor, MI 48109, USA*

[*]*ijov@umich.edu*

Abstract: Ultrafast mid-infrared (IR) coherent radiation plays an important role in strong-field physics, wherein the use of longer wavelengths has reduced the optical intensities needed to drive light-matter interactions by orders of magnitude in comparison to near-IR radiation. Optimizing parametric interactions for generation and characterization of mid-IR pulses is an enabling step for those applications. We report on the production of $>$50 μJ femtosecond pulses centered at 5 μm in a two-stage optical parametric amplifier (OPA) based on $ZnGeP_2$, a high-performance optical material in this spectral region. The OPA is pumped by an ultrafast 2-μm source. Amplified pulses have been characterized by parametric upconversion, enabling the use of standard silicon detectors. A numerical model of the system has been developed and tested to control dispersion, group-velocity mismatch, and off-axis parametric fluorescence. The source architecture is suitable for production of mJ-level mid-IR ultrafast pulses without the use of chirped-pulse amplification, where convenient pumping could be realized directly by mid-IR laser sources based on materials such as Cr:ZnSe or Cr:ZnS.

OCIS codes: (320.7110) Ultrafast nonlinear optics; (190.4970) Parametric oscillators and amplifiers.

References and links

1. S. A. Diddams, L. Hollberg, and V. Mbele, "Molecular fingerprinting with the resolved modes of a femtosecond laser frequency comb," Nature **445**, 627–630 (2007).
2. A. Schliesser, N. Picqué, and T. W. Hänsch, "Mid-infrared frequency combs," Nat. Photonics **6**, 440–449 (2012).
3. M.-C. Chen, P. Arpin, T. Popmintchev, M. Gerrity, B. Zhang, M. Seaberg, D. Popmintchev, M. M. Murnane, and H. C. Kapteyn, "Bright, coherent, ultrafast soft x-Ray harmonics spanning the water window from a tabletop light source," Phys. Rev. Lett. **105**, 173901 (2010).
4. T. Popmintchev, M. C. Chen, D. Popmintchev, P. Arpin, S. Brown, S. Ališauskas, G. Andriukaitis, T. Balčiūnas, O. D. Mucke, A. Pugžlys, A. Baltuška, B. Shim, S. E. Schrauth, A. Gaeta, C. Hernandez-Garcia, L. Plaja, A. Becker, A. Jaron-Becker, M. M. Murnane, and H. C. Kapteyn, "Bright coherent ultrahigh harmonics in the keV X-ray regime from mid-infrared femtosecond laser," Science **336**(6086), 1287–1291 (2012).
5. G. G. Paulus, W. Becker, W. Nicklich, and H. Walther, "Rescattering effects in above-threshold ionization: a classical model," J. Phys. B: At. Mol. Opt. Phys. **27**, L703–L708 (1994).

#258356 Received 28 Jan 2016; revised 22 Feb 2016; accepted 25 Feb 2016; published 2 Mar 2016

6. J. L. Krause, K. J. Schafer, and K. C. Kulander, "High-order harmonic generation from atoms and ions in the high intensity regime," Phys. Rev. Lett. **68**, 3535 (1992).
7. G. Tempea, M. Geissler, M. Schnürer, and T. Brabec, "Self-phase-matched high harmonic generation," Phys. Rev. Lett. **84**, 4329 (2000).
8. S.-W. Huang, G. Cirmi, J. Moses, K.-H. Hong, S. Bhardwaj, J. R. Birge, L.-J. Chen, E. Li, B. J. Eggleton, G. Cerullo, and F. X. Kärtner, "High-energy pulse synthesis with sub-cycle waveform control for strong-field physics," Nat. Photonics **5**, 475–479 (2011).
9. P. Moulton and E. Slobodchikov, "1-GW-peak-power, Cr:ZnSe laser," in *Proceedings of CLEO:2011–Laser Applications to Pho-tonic Applications*, OSA Technical Digest (CD), paper PDPA10 (2011).
10. N. Tolstik, E. Sorokin, and I. Sorokina, "Kerr-lens mode-locked Cr:ZnS laser," Opt. Lett. **38**(3), 299–301 (2013).
11. F. Stutzki, F. Jansen, C. Jauregui, J. Limpert and A. Tünnermann, "2.4 mJ, 33 W Q-switched Tm-doped fiber laser with near diffraction-limited beam quality," Opt. Let. **38**(2), 97–99 (2013).
12. E. J. Takahashi, T. Kanai, Y. Nabekawa, and K. Midorikawa, "10 mJ class femtosecond optical parametric amplifier for generating soft x-ray harmonics," Appl. Phys. Lett. **93**, 041111 (2008).
13. C. Li, D. Wang, L. Song, J. Liu, C. Xu, Y. Leng, R. Li, and Z. Xu, "Generation of carrier-envelope phase stabilized intense 1.5 cycle pulses at 1.75 μm," Opt. Express **19**(7), 6783-6789 (2011).
14. R. Agustsson, E. Arab, A. Murokh, B. O'Shea, A. Ovodenko, I. Pogorelsky, J. Rosenzweig, V. Solovyov, and R. Tilton, "Measuring single-shot, picosecond optical damage threshold in Ge, Si, and sapphire with a 5.1-μm laser," Opt. Mat. Express **5** 2835–2842 (2015).
15. B. Naranjo, A. Valloni, S. Putterman, and J. Rosenzweig, "Stable charged-particle acceleration and focusing in a laser accelerator using spatial harmonics," Phys. Rev. Lett. **109**, 164803 (2012).
16. G. Andriukaitis, T. Balčiūnas, S. Ališauskas, A. Pugžlys, A. Baltuška, T. Popmintchev, M.-C. Chen, M. Murnane, and H. Kapteyn, "90 GW peak power few-cycle mid-infrared pulses from an optical parametric amplifier," Opt. Lett. **36**(15), 2755–2757 (2011).
17. V. Petrov, F. Rotermund, F. Noack, and P. Schunemann, "Femtosecond parametric generation in $ZnGeP_2$," Opt. Lett. **24**(6), 414–416 (1999).
18. F. Rotermund, V. Petrov, and F. Noack, "Difference-frequency generation of intense femtosecond pulses in the mid-IR (4-12 μm) using $HgGa_2S_4$ and $AgGaS_2$," Opt. Commun. **185**, 177–183 (2000).
19. F. Seifert, V. Petrov, and M. Woerner, "Solid-state laser system for the generation of mid-infrared femtosecond pulses tunable from 3.3 to 10 μm," Opt. Lett. **19**(23), 2009–2011 (1994).
20. V. Petrov, V. Badikov, G. Shevyrdyaeva, V. Panyutin, and V. Chizhikov, "Phase-matching properties and optical parametric amplification in single crystals of $AgGaGeS_4$," Opt. Mat. **26**(3), 217–222 (2004).
21. K. Vodopyanov, "Broadly and fast tunable optical parametric oscillator," U.S. patent 20110261438 (2011).
22. S. Das, G. C. Bhar, S. Gangopadhyay, and C. Ghosh, "Linear and nonlinear optical properties of $ZnGeP_2$ crystal for infrared laser device applications: revisited," Appl. Opt. **42**(21), 4335–4340 (2003).
23. Y. C. Yin, D. French, and I. Jovanovic, "Ultrafast temporal pulse shaping via phase-sensitive three-wave mixing," Opt. Express **18**(17), 18471–18482 (2010).
24. Y. R. Shen, *The Principle of Nonlinear Optics* (Wiley, 2003).
25. M. D. Feit and J. A. Fleck, Jr., "Computation of mode properties in optical fiber waveguides by a propagating beam method," Appl. Opt. **19**(7), 1154–1164 (1980).
26. M. N. Cizmeciyan, H. Cankaya, A. Kurt, A. Sennaroglu, "Operation of femtosecond Kerr-lens mode-locked Cr:ZnSe lasers with different dispersion compensation methods," Appl. Phys. B **106**(4), 887–892 (2012).
27. G. Xu, S. Wandel, and I. Jovanovic, "Nondegenerate parametric generation of 2.2-mJ, few-cycle 2.05-μm pulses using a mixed phase matching scheme," Rev. Sci. Instrum. **85**, 023102 (2014).
28. S. Wandel, G. Xu, Y. Yin, and I. Jovanovic, "Parametric generation of energetic short mid-infrared pulses for dielectric laser acceleration," J. Phys. B: At. Mol. Opt. Phys. **47**, 234016 (2014).
29. G. Cerullo and S. De Silvestri, "Ultrafast optical parametric amplifiers," Rev. Sci. Instrum. **74**, 1–18 (2003).

1. Introduction

The generation and application of tunable femtosecond pulses in the mid-infrared (IR) spectral region has greatly expanded the reach of existing optical techniques that use near-IR driving wavelengths, such as molecular fingerprinting [1], frequency combs [2], and high-harmonic generation (HHG) [3]. Inorganic and organic molecules show the strongest absorption features associated with fundamental vibrational resonances in the mid-IR part of the spectrum. Understanding the vibrational dynamics in these systems is limited by the lack of commercial lasers with spectral coverage in the mid-IR region that have sufficiently short pulse durations or high pulse energies needed to probe their molecular environments. Sub-ps-level pulse durations in the mid-IR region are needed to resolve the fast dephasing times of stretching vibrations in dif-

#258356 Received 28 Jan 2016; revised 22 Feb 2016; accepted 25 Feb 2016; published 2 Mar 2016

ferent molecular bonds of interest, such as O–H and N–H. Therefore, a technological gap exists in production of ultrashort, high-energy mid-IR laser pulses that would be suitable for mid-IR spectroscopy.

HHG in molecules subjected to a tunable mid-IR laser field around the vibrational resonance is more sensitive to the driving laser wavelength than that in atoms with comparable ionization potential as a result of the vibrational motion in molecules. Using a long-wavelength driving laser pulse makes it possible to generate shorter wavelength high harmonics due to the quadratic ponderomotive energy scaling with laser wavelength. The scaling of the harmonic cutoff has been demonstrated recently with high-energy mid-IR pulses, resulting in attosecond pulse generation via HHG [4]. To date, the vast majority of HHG studies using mid-IR driving lasers are purely theoretical, either because the short-duration driving laser pulses needed are difficult to generate reliably, or because the pulse energies required are unattainable at longer wavelengths. There is a strong motivation to produce intense, ultrashort mid-IR laser pulses that can be used to better understand the wavelength scaling of physical processes in important molecules.

Within the tightly localized ionization region produced by an intense laser pulse, some of the liberated electrons are re-scattered on the ion core, leading to above-threshold-ionized electron acceleration to kinetic energies of up to $10U_P + I_P$ [5] and, in the case of electron-core recombination, HHG with photon energies of up to $3.17U_P + I_P$ [6]. Here, I_P denotes the atom's ionization potential and $U_P = E^2/4\omega^2$ refers to the ponderomotive potential. It is evident that both an increase in the drive pulse intensity and its wavelength can help generate high harmonics. The use of longer-wavelength drive pulses has resulted in improved phase matching in HHG [7, 3]. In addition, few-cycle mid-IR driving laser pulses reduce depletion of the neutral gas target by ionization before the main peak of the electric field, generating high-energy XUV photons [8].

Current laser technology for the mid-IR region is severely limited, as most of the recent progress in laser science has been made in the near-IR part of the spectrum. The present paradigm for ultrafast mid-IR production is heavily biased towards near-IR-pumped optical parametric (chirped-) pulse amplification (OPA and OPCPA). Advances have been made in mode-locked crystalline solid-state lasers and fiber oscillators based on Cr^{2+}-doped chalcogenides, such as Cr:ZnSe [9] and Cr:ZnS [10], and Tm^{3+}-doped fiber lasers [11], respectively, but these technologies are not optimally suited for high-pulse-energy applications such as HHG. Near-IR-pumped mid-IR OPA/OPCPA is scalable to high average power, but has low wall-plug efficiency and cannot take advantage of the nonlinear optical materials with the most attractive properties for mid-IR pulse production, which require mid-IR pump lasers. Nonetheless, parametric systems represent the most viable path for near-term advancement of mid-IR sources, especially when tunability is sought. While many of the proposed and demonstrated schemes to date are scalable to higher energies, they frequently rely on complex and unique pump lasers and system designs that incorporate multiple lasers, especially for OPCPA. OPAs have also been used for production of high-energy, ultrashort pulses; however, the lack of output stability [12] and highly modulated beam profiles [13] present issues for many intended applications. Ultrafast OPAs often operate near degeneracy to realize high gain and broad bandwidth. Even when operated closer to degeneracy, three stages of amplification are usually required to obtain high energies. It is desirable to use a crystal with a large nonlinear coefficient to reduce the size and complexity of an OPA while simultaneously achieving high parametric gain.

In this paper, we model and experimentally demonstrate an approach for production of high-energy ultrashort mid-IR laser pulses at a center wavelength of 5 μm designed to take advantage of mid-IR pumping by 2–2.5-μm pump lasers, such as the Cr:ZnSe laser. The objective of this work is to develop an energy-scalable design delivering few-cycle pulses near 5 μm with a pulse energy at a mJ level. The target mid-IR pulse energy level is determined by experimental

#258356 Received 28 Jan 2016; revised 22 Feb 2016; accepted 25 Feb 2016; published 2 Mar 2016

optical damage threshold measurements at 5.3 μm from a frequency-doubled CO_2 laser in an effort to avoid field breakdown in silicon microstructures [14], which could be used to support direct laser acceleration, another important application of this type of source [15]. The required diagnostics for comprehensive characterization of this type of source is unavailable from commercial sources or has even not been demonstrated to date. The unique challenge associated with the temporal characterization is operation in the few-cycle regime in the mid-IR part of the spectrum. This necessitates the development of a suitable characterization technique, such as cross-correlation with a short reference pulse. Our parametric source utilizes the mature Ti:sapphire laser pump technology to develop a surrogate 2-μm pump and a 5-μm mid-IR source. A two-stage OPG/OPA pumped in the mid-IR producing 700-fs pulses, with a pulse energy of 120 μJ (signal + idler) and excellent shot-to-shot energy stability, is presented. The temporal properties of these pulses are characterized using cross-correlation with a standard, Si-based, CCD detector. This design will allow the development of a new class of efficient parametric sources at 5 μm and beyond based on high-nonlinearity materials that take advantage of novel mid-IR laser pump sources under development.

2. Design considerations

Direct pumping with near-IR pump pulses produce mid-IR pulses is possible with some crystals; however, the transparency range and ability to achieve phase matching is typically limited to <4 μm. Production of longer wavelengths requires different nonlinear media, such as $ZnGeP_2$ (ZGP), $AgGaS_2$ (AGS), or GaSe, which themselves require mid-IR (>2-μm) pumping. Short pump pulses near 2 μm can be produced either directly from a mid-IR laser (such as Cr:ZnSe or Cr:ZnS) or with a suitable parametric source. β-BaB_2O_4 borate (BBO) and BiB_3O_6 (BiBO) are frequently used for parametric generation of mid-IR pulses using near-IR pumps; however, both are limited to wavelengths $\lesssim$2 μm due to crystal transparency. $KTiOAsO_4$ (KTA) has been used to produce 8-mJ few-cycle pulses near 3.9 μm in an OPCPA scheme [16] but is not transparent at wavelengths $\gtrsim$4 μm. Operation at longer wavelengths requires the use of different materials with more favorable characteristics for short mid-IR pulse production. In ZGP pumped at 2 μm by the idler beam of a 800-nm pumped OPA, tuning from 2.5 to 10 μm was demonstrated [17]. Maximum energies of 9 μJ near 4 μm and >1 μJ in the entire tuning range up to 12 μm were reported [18], where $HgGa_2S_4$ (HGS) was used as a nonlinear crystal. Tunable mid-IR pulse generation through difference-frequency generation (DFG) between the signal and the idler pulses of a 800-nm pumped OPA is commonly achieved with AGS, which allows continuous tuning from 2.4 μm to wavelengths longer than 12 μm [19]. To characterize parametric interaction and compare different nonlinear materials, it is useful to define parametric gain as a figure of merit:

$$\mathrm{FOM} = \frac{I_s(L_c)}{I_{s0}} = \frac{1}{4}\exp(2\Gamma L_c), \tag{1}$$

which describes the parametric gain growing exponentially with crystal length L_c and with nonlinear coefficient Γ, given as

$$\Gamma^2 = \frac{8\pi^2 d_{\mathrm{eff}}^2 I_p}{n_i n_s n_p \lambda_i \lambda_s \varepsilon_0 c_0}, \tag{2}$$

where d_{eff} is the effective nonlinearity, I_p is the pump intensity, $n_{i,s,p}$ are the refractive indices of the idler, signal, and pump wavelengths, respectively, $\lambda_{i,s}$ are the wavelengths of the idler and signal, respectively, ε_0 is the vacuum permittivity, and c_0 is the speed of light in vacuum. Several of the commonly used crystals for mid-IR pulse generation are characterized by this

#258356 Received 28 Jan 2016; revised 22 Feb 2016; accepted 25 Feb 2016; published 2 Mar 2016

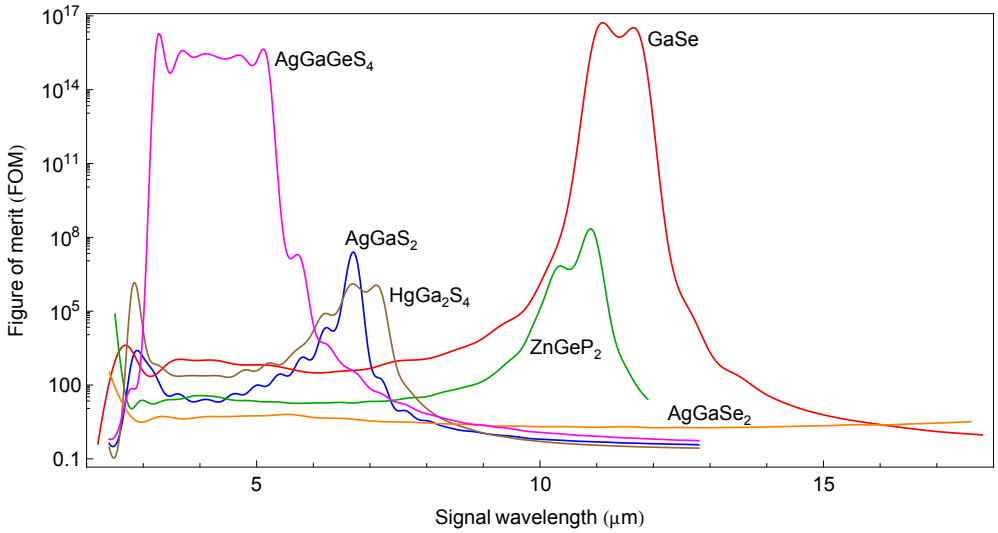

Fig. 1. Calculated figure of merit (parametric gain) for several commonly used crystals for mid-IR pulse generation. The pump intensity used for calculations is 1.1 GW/cm^2. The crystal length used is equal to the pulse splitting length for each phase-matching condition ($\lambda_p = 2.05$ μm), using a pump pulse duration of 60 fs.

figure of merit in Fig. 1 for the conditions representative of our setup ($\lambda_p = 2.05$ μm) for a crystal length equal to the pulse splitting length, l_{sp}.

All of the mid-IR crystals considered in this study are uniaxial, exhibiting a combination of advantages and drawbacks that depend on the exact application. AGS and AGSe have low residual absorption, but exhibit poor thermal conductivity and experience anisotropic thermal expansion. ZGP has excellent nonlinearity and thermal conductivity but multi-phonon and residual absorption limit its transparency so that pump wavelengths $\gtrsim$2 μm are needed, corresponding to $<$1/3 of its bandgap. HGS has a high FOM, but it is challenging to grow, making only small crystal sizes available. GaSe and $AgGaGeS_4$ exhibit large nonlinearities and birefringence, but have low damage thresholds, effectively limiting the pump intensity and reducing the conversion efficiency that can be achieved [20]. ZGP is a highly attractive candidate for our intended operation space due to its high effective nonlinearity (77.3 pm/V for our phase matching conditions), broad transparency range (2–12 μm), and high damage threshold ($>$300 MW/cm^2). However, due to two-photon absorption at near-IR wavelengths, ZGP must be pumped in the mid-IR region.

The two-stage OPA mid-IR source that pumps the ZGP OPA presently serves as a surrogate source for mid-IR pumping, which can be replaced by direct pumping with one of the developing mid-IR laser technologies, such as Cr:ZnSe. The surrogate source used to pump the 5-μm OPA generates laser pulses centered at a wavelength of 2.05 μm. Pumping near the degeneracy wavelength (2.5 μm) would greatly reduce the GVM, as shown in Fig. 2(a), enabling the use of longer crystals for amplification, as determined by the effective interaction length. Broad, nearly level regions of GVM exist when pumping with λ_p =2.5, 2.05, 1.9, or 1.75 μm. This result indicates that type I phase matching has the potential to produce broad bandwidth pulses across a wide tuning range. This represents a prerequisite for the generation of bandwidth-limited femtosecond pulses over a broad spectral region. Pumping near the degeneracy also increases the effective nonlinearity, which becomes nearly constant over a broad

#258356 Received 28 Jan 2016; revised 22 Feb 2016; accepted 25 Feb 2016; published 2 Mar 2016

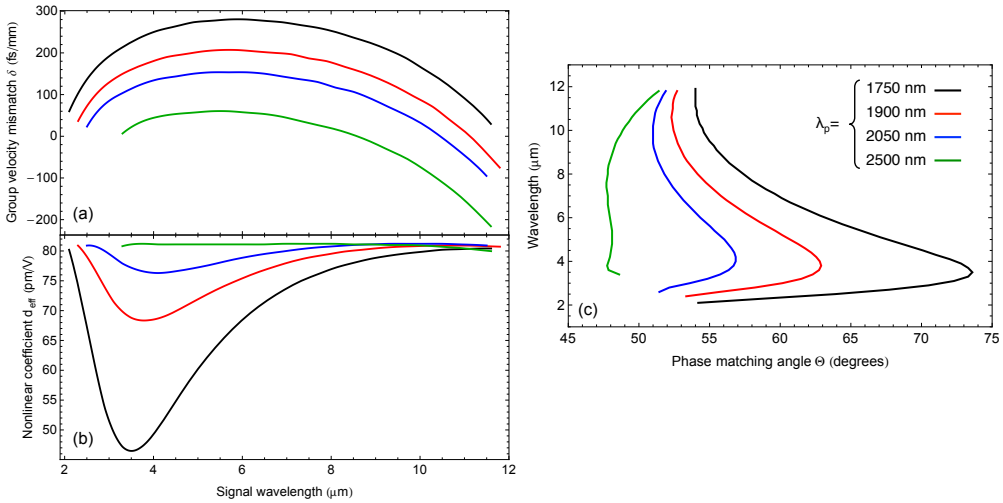

Fig. 2. (a) Calculated GVM, (b) nonlinear optical coefficient, and (c) phase-matching angle in a type-I ZGP crystal for a 5-μm idler wavelength with a pump wavelength of λ_p=1.75 μm (black), λ_p=1.90 μm (red), λ_p=2.05 μm (blue), and λ_p=2.50 μm (green).

range of signal wavelengths with a pump wavelength of $\lambda_p = 2.5$ μm, as shown in Fig. 2(b), allowing for efficient amplification across a broad spectral range. Figure 2(c) shows the potential tuning range (signal and idler) for type I phase matching by use of several near-IR pump wavelengths. It is well-known that the largest achievable gain bandwidth for parametric processes occurs when the GVD of the nonlinear crystal pumped at degeneracy is close to zero for the signal/idler wavelength [21]. By pumping near the degeneracy wavelength (λ_p=2.5 μm), the entire tuning range can be accessed by adjusting the crystal angle over a range of $<5^\circ$. For this calculation we used the Sellmeier parametrization from Ref. [22].

3. Numerical modeling for a plane-wave phase-insensitive OPA

A one-dimensional three-wave mixing numerical model was used to examine the influence of pump/seed quadratic temporal phase (chirp) on the OPA by modifying the previously developed model [23] for the mixing process described herein. In this study, the following assumptions and simplifications are made: (1) the mixing process is collinear, (2) the three mixing waves exist in a single spatial mode (plane wave), but are longitudinally multimode, (3) the nonlinear medium exhibits no linear or nonlinear absorption, and (4) there is no cross phase modulation. The model uses standard coupled differential equations with the slowly varying amplitude approximation ($|d^2A/dz^2| \ll |k\, dA/dz|$) for three-wave mixing [24], which can be written as

$$\frac{dA_1(z)}{dz} = i\frac{2d_{\text{eff}}\omega_1^2}{k_1c^2}A_2^*(z)A_3(z)\exp(i\Delta kz) \tag{3}$$

$$\frac{dA_2(z)}{dz} = i\frac{2d_{\text{eff}}\omega_2^2}{k_2c^2}A_1^*(z)A_3(z)\exp(i\Delta kz) \tag{4}$$

$$\frac{dA_3(z)}{dz} = i\frac{2d_{\text{eff}}\omega_3^2}{k_3c^2}A_1(z)A_2(z)\exp(i\Delta kz), \tag{5}$$

where $A_{1,2,3}$ are the complex field amplitudes of the idler, signal, and pump waves, respectively, d_{eff} is the effective nonlinearity, ω_i is the angular frequency, k_i is the wave vector, $\Delta k = k_3 -$

#258356 Received 28 Jan 2016; revised 22 Feb 2016; accepted 25 Feb 2016; published 2 Mar 2016

$k_2 - k_1$ is the wave vector mismatch, and c is the speed of light in vacuum. The longitudinal coordinate is denoted by z. To address the important temporal characteristics of this process, the complex amplitude of the idler, signal, and pump pulses A_i are represented in the time and frequency domain: $A_i = A_i(t) = \mathscr{F}^{-1}[A_i(\omega)]$, including the corresponding amplitude and phase.

While the nonlinear mixing process is described in the time domain, dispersion is more readily represented in the spectral domain. Dispersion is included in the model using the usual split-step approach [25], by transforming the fields into the spectral domain after each step of numerical integration in the time domain. The spectral phase applied to the three fields at each step is

$$A_i(\omega) \rightarrow A_i(\omega)\exp(i n_i(\omega)\omega/c), \tag{6}$$

where ω is the angular frequency and $n(\omega)$ is the refractive index for the corresponding spectral component ω of A_i. Self-phase modulation is included in the model by applying the temporally-dependent phase to each wave

$$A_i(t) \rightarrow A_i(t)\exp\left(i n_2^{NL}\omega_i I_i(t) dz/c\right), \tag{7}$$

where n_2^{NL} is the Kerr nonlinear refractive index (from Ref. [22]), I_i(t) is the instantaneous intensity at time t, and ω_i is the center frequency of wave A_i. The incident idler, seed (signal), and pump beams are centered at 5 μm, 3.47 μm, and 2.05 μm, respectively. While there is no incident idler pulse, the incident seed and pump pulses are assumed to have a Gaussian spectral profile with a spectral bandwidth chosen such that their initial transform-limited pulse duration is 100 fs. Phase matching is achieved by orienting the ZGP crystal at 56.1° measured from its principal axis, as shown in Fig. 2(c).

For ultrashort laser pulses, GVM plays a critical role in determining the magnitude of gain achievable in the OPA process by setting the pulse splitting length. GVM in crystals longer than the pulse splitting length can also introduce modulation on the interacting pulses after they separate in time. Our model includes this consideration, as seen in Fig. 3(a), owing to the pump and signal walking away from one another after the pulse splitting length [$l_{sp} = L_c/2$ for case (a)]. Beyond this length, additional crystal length does not produce useful parametric gain. Increasing the pulse-splitting length also increases the pump pulse duration, so that the signal and pump remain overlapped in time over a greater distance. This is shown in Fig. 3(a), where the pump and idler time profiles are modeled as they propagate over the length of the ZGP crystal. From the first visualization in Fig. 3(a), it is evident that the pump and signal pulses walk away from each other at a distance equal to the pulse splitting length, which is half of the length of the 1.5-mm crystal used in our experiment. Beyond this length, gain is not present and pump depletion is low. Figure 3(b) represents the case where the pump pulse is stretched, thereby increasing the pulse splitting length and allowing amplification to occur over the entire length of the crystal. Proper dispersion management is also needed that can identify sources of dispersion within the OPA design to determine the pump pulse duration at each OPA stage. If instead the OPA is pumped near degeneracy for 5-μm production ($\lambda_p = 2.5$ μm), the GVM between the interacting waves is reduced, leading to an increase of the pulse splitting length. The proposed pump laser host (Cr:ZnSe) is capable of producing pulses near 2.5 μm with a duration as short as 92 fs [26]. Even without additional pump pulse stretching, using this pump laser would result in a pulse splitting length that is longer than the length of the OPA crystal currently in use, such that GVM effects could be neglected.

4. Source architecture

A schematic of the constructed two-stage ZGP OPA is shown in Fig. 4. The OPA was pumped with ∼60-fs, 1.6-mJ pulses at 2.05-μm from a two-stage OPA based on BBO crystals [27],

#258356 Received 28 Jan 2016; revised 22 Feb 2016; accepted 25 Feb 2016; published 2 Mar 2016

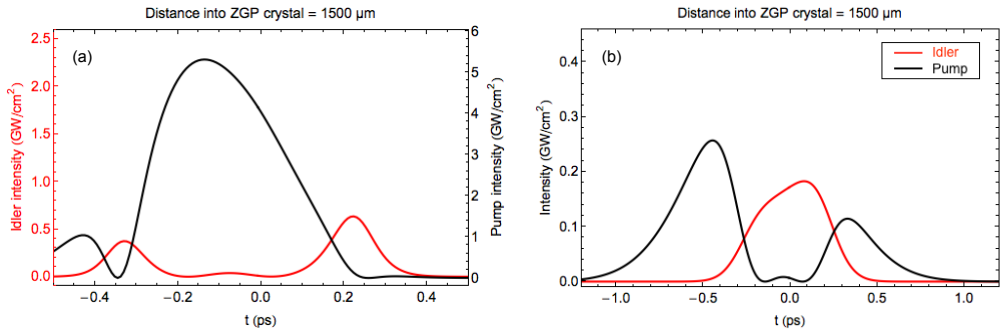

Fig. 3. Temporal pulse evolution for pump (black) and idler (red) waves as they traverse the nonlinear medium for a pulse splitting length equal to (a) 1/2 L_c (see Visualization 1) and (b) L_c (see Visualization 2).

which was in turn pumped by a commercial Ti:sapphire chirped-pulse amplification system (Trident X, Amplitude Technologies) that supplies 40-fs, 14-mJ laser pulses centered at 800 nm with a repetition rate of 10 Hz. Approximately 25 μJ of pump energy was focused onto a 1-mm-thick ZGP crystal to produce optical parametric generation (OPG). Each ZGP crystal used in the optical setup was cut at an angle of $\theta_m = 56.1^\circ$ for type I phase matching. The lens L3 was chosen to maximize the pump pulse intensity without exceeding the damage threshold of ZGP, previously reported to have a lower limit surface damage threshold for femtosecond pulses of 100 GW/cm^2 [17]. We observe a parametric fluorescence cone after propagation through the OPG crystal when a pump intensity >35 GW/cm^2 is used. At higher incident intensities, the generated OPG signal energy diminishes as a result of non-phase-matched second-harmonic generation. We have also considered the use of self-phase modulation for seed pulse production; however, under identical pumping conditions, OPG produced higher seed pulse energy with better energy stability. The OPG pulse is subsequently collimated using L4 and filtered using a long-wave-pass (LP) 3000-nm filter to remove the residual pump energy. The 3.47-μm OPG is then stretched in a 5-mm-thick germanium plate, enabling selective amplification of different portions of the OPG spectrum in the subsequent OPA by adjusting the seed-pump delay. OPGs exhibit temporal incoherence; however, the coherence is enhanced subsequent to OPG by chirping the OPG pulse and selecting a small temporal/spectral portion of the stretched OPG pulse for frequency mixing in the first OPA [28]. The stretcher also serves to block any residual pump energy and improve parametric amplification of the seed in the first OPA stage. The OPG is directed to the first OPA crystal via a delay line and interacts with the pump beam at an angle of 4.6°. Locating the angle of maximum amplification was performed by overlapping the seed beam with the area of largest gain as observed from the parametric fluorescence cone present when only the pump beam is incident onto the crystal. The use of a noncollinear geometry allows for spatial separation of the preamplified signal beam from the residual pump and idler beams without the need for dichroic filters. The preamplified signal beam at 3.47 μm is then sent to the second OPA crystal after recombining with the pump beam on a dichroic mirror (DM1).

In OPAs that operate away from degeneracy, it is advantageous to use noncollinear phase matching, which can dramatically increase the gain bandwidth [29]. By injecting the pulse with a higher group velocity at a certain angle, α, relative to normal incidence from the crystal, the group velocity projection onto the second pulse matches the group velocity of the first and broadband phase matching is realized along the entire crystal length. In a type I ZGP OPA pumped at λ_p=2.05 μm for a signal wavelength λ_s=3.47 μm, broadband phase matching is

#258356 Received 28 Jan 2016; revised 22 Feb 2016; accepted 25 Feb 2016; published 2 Mar 2016

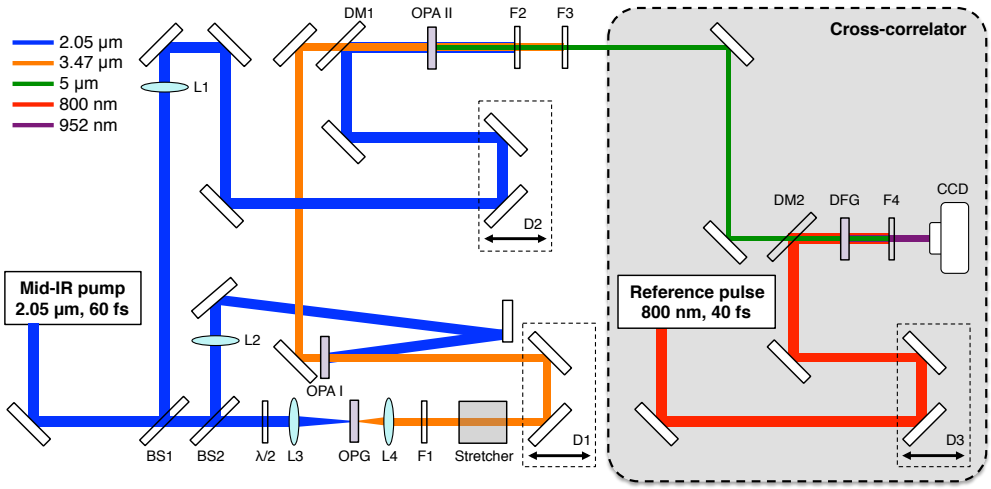

Fig. 4. Schematic of mid-IR OPA and scanning cross-correlator. BS: beamsplitter, $\lambda/2$: half-waveplate, L: lens, F1: LP 3000-nm filter, F2: LP 2500-nm filter, F3: LP 4500-nm filter, F4: BP 950−40-nm filter, DM: dichroic mirror, D: delay, OPG: 1.5-mm ZGP crystal, OPA I: 1.0-mm ZGP crystal, OPA II: 1.5-mm ZGP crystal, DFG: 1.0-mm MgO:$LiNbO_3$ crystal, CCD: silicon charge-coupled device (Mightex).

achieved for $\alpha = 2.3^\circ$. For a collinear scheme ($\alpha = 0^\circ$), the phase-matching angle strongly depends on the signal wavelength, and phase matching can only be achieved over a narrow spectral range for a fixed crystal orientation. The central wavelength of the mid-IR output could be tuned from 4500 to 5600 nm by adjusting the temporal overlap of the OPG and pump pulses and slightly modifying the OPA crystal angle to achieve phase-matching.

Temporal characterization of the mid-IR output of the OPA was accomplished by DFG cross-correlation measurements using a small portion of the unconverted 800-nm pump from the 2-µm OPA system. 800-nm pulses serve as a reference pulse, having been fully characterized previously by spectral interferometry for direct E-field reconstruction (SPIDER). The 5-µm mid-IR output and the 800-nm reference pulse combine collinearly on a dichroic mirror (DM2) and mix in a 1-mm-thick MgO:$LiNbO_3$ crystal cut at an angle of $\theta_m = 46.2^\circ$ for DFG. The cross-correlation signal at 952 nm is imaged onto a silicon CCD after passing through a bandpass filter to remove residual pump energy. Spectral properties of the cross-correlation signal were also measured by imaging the light onto a single-shot near-IR spectrometer (Mightex). A delay line was used to scan the temporal overlap of the two beams to obtain a cross-correlation trace.

5. Experimental results

The spectra of 5-µm idler pulses and 3.47-µm signal pulses emerging from the OPG and OPA stages were collected by a 20-cm uncoated CaF_2 lens and analyzed using a 0.55-m monochromator with a 300-mm^{-1} grating blazed at 4 µm, in combination with a thermoelectrically cooled InSb photodetector with an upper wavelength detection limit of 6 µm. The measured and calculated pulse spectra are shown in Fig. 5. The measured spectra from the preamplification (OPA I) and the power-amplification (OPA II) stages of the OPA setup are in close agreement with the calculated spectra from our numerical model. The OPG signal (shown in purple) was measured after inserting a LP 3000-nm filter to remove residual pump energy from the OPG stage. The signal beam from the preamplification stage (shown in orange) used to seed the second OPA

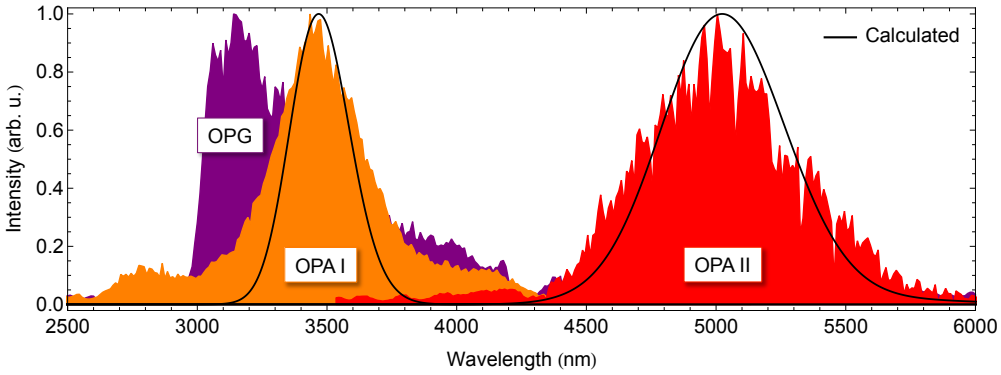

Fig. 5. Normalized measured and calculated pulse spectra emerging from each amplification stage. Purple: OPG after passing through 1.5-mm ZGP crystal measured with a LP 3000-nm filter; orange: preamplified seed after passing through 1.0-mm ZGP crystal; red: amplified idler after passing through 1.5-mm ZGP crystal. Calculated spectra are shown with solid black lines.

is centered at a wavelength of 3470 nm, and the amplified idler beam (shown in red) from the second OPA stage is centered at a wavelength of 5000 nm. The measured spectrum from the preamplification stage is slightly broader than the calculated spectrum, owing to higher-order dispersion terms in the signal beam path that cannot be compensated with material dispersion. It is well-known that the use of noncollinear interaction angles translates to spatial chirp of the idler in OPAs [29]. As a result, we estimate the resulting spatial chirp of order 200 nm across the beam profile of the 5 μm idler, *i.e.* the shift of center wavelength by 4% of the center wavelength from one edge of the beam to another, corresponding to 27% of the bandwidth. The equivalent angular dispersion is 0.17 mrad. Using this source design, dispersion management is relatively straightforward and necessary only in the final OPA stage and thereafter.

Energy measurement of the pump, signal, and idler pulses have been conducted using a pyroelectric detector, providing a sensitivity of ∼20 nJ. With the described source design, the idler pulses produced have a pulse energy of 53 μJ with an rms energy stability of 1.8% measured over 600 shots, as shown in Fig. 6(b). Local (spatial/temporal) depletion of the pump in the OPA II stage results in a significant pulse energy stability improvement when compared to the OPG stage. The crystal orientation in the OPA II stage was adjusted to improve the beam quality of the idler pulses, incurring some penalty in the output energy from the OPA [Fig. 6(b), inset].

6. Difference-frequency generation cross correlation

Pumping short-pulse OPAs in the mid-IR enables production of longer-wavelength laser pulses not attainable with near-IR-pumped nonlinear crystals, but also creates new constraints on materials used. This is largely due to material absorption within the mid-IR spectral region, but atmospheric absorption can also be present. Additionally, the low energy of mid-IR photons means that ubiquitous silicon-based charge-coupled device (CCD) detectors cannot be used. Longer-wavelength laser pulse characterization commonly relies on non-self-referencing methods, such as cross-correlation, that use a known, higher-intensity pulse to diagnose pulses indirectly by producing a higher-intensity, higher-frequency signal that can be measured through the use of standard silicon detectors, which are sensitive up to around 1100 nm. Cross-correlation is simple in practice because it, like OPA, does not require spatial coherence or mode-matching for its

#258356 Received 28 Jan 2016; revised 22 Feb 2016; accepted 25 Feb 2016; published 2 Mar 2016

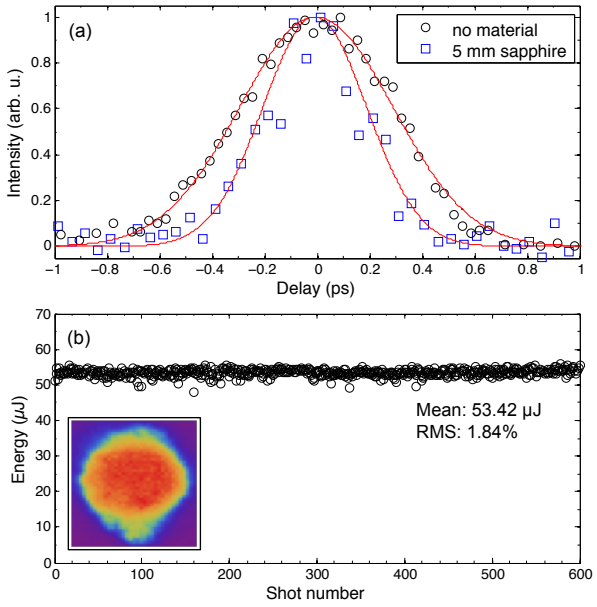

Fig. 6. (a) Amplified idler pulse duration before (black circles) and after (blue squares) adding 5-mm-thick sapphire window measured by scanning cross-correlation in a MgO:$LiNbO_3$ crystal and best-fit Gaussian distribution (red). (b) Energy stability of 5-µm idler pulses; inset: far-field beam profile of amplified 5-µm pulse measured by an InSb array camera.

implementation. We used unconverted 800-nm light as a reference to produce a 952-nm DFG cross-correlation signal with our unknown 5-µm pulse in a 1-mm-thick MgO:$LiNbO_3$ crystal. The DFG signal wavelength can be detected with a silicon detector and the central wavelength is sufficiently far from that of the reference pulse to selectively remove the reference from the DFG signal with the addition of dichroic filters. The 800-nm reference pulse has previously been characterized using SPIDER, and the 40-fs pulse duration is sufficiently short compared to the 5-µm pulse duration that we estimate by scanning the delay of the second OPA stage with the short 2-µm pump source.

Numerical modeling of the difference-frequency mixing process shows that the difference-frequency pulse amplitude closely matches the amplified pulse, mainly because the reference pulse is considerably shorter than the amplified pulse duration. MgO:$LiNbO_3$ was chosen as the nonlinear crystal for DFG due to its excellent transparency and small GVM for the three interacting waves. Using a 40-fs pump pulse duration, the pulse splitting length was calculated to be ~3.5-mm, so GVM effects can be neglected for this measurement. We use collinear interaction to avoid any distortions caused by mixing chirped pulses nonlinearly in parametric interaction. 5-µm photons are not energetic enough to generate response on the silicon CCD. Temporally resolving the signal was done by scanning a delay stage using an encoded motorized actuator with a time step resolution of 0.33 fs. Using this method, we are able to measure temporal features of the amplified mid-IR pulses accurately with a standard CCD sensitive to visible and near-IR radiation. The 5-µm pulses have a full-width at half-maximum pulse duration of 700 fs, as shown in Fig. 6(a).

The importance of quantifying the spectral phase stems from the usual requirement for high fidelity recompression of the amplified pulses in chirped-pulse amplification. Since the recom-

#258356 Received 28 Jan 2016; revised 22 Feb 2016; accepted 25 Feb 2016; published 2 Mar 2016

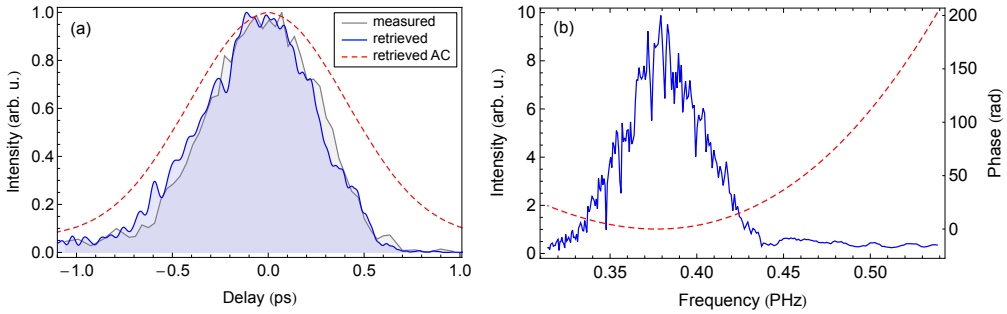

Fig. 7. (a) Measured (gray), calculated (blue), and calculated AC (red dashed) time profiles of amplified 5-μm pulses; (b) measured pulse spectrum (blue) and retrieved spectral phase (red dashed) of amplified idler pulses.

pressed pulse is determined not only by the spectral amplitude bandwidth, but also by the spectral phase, it is important to identify the contributions to the spectral phase in the system. Spectral phase of the amplified idler pulses was calculated from a combination of the measured cross-correlation time profile and the measured spectrum, as shown in Fig. 7. An iterative process for spectral phase retrieval was used by truncating the terms after third-order dispersion (TOD) due to the fact that the importance of reconstruction of higher-order terms of dispersion is reduced for longer pulses. Retrieval results show that the reconstructed pulse amplitude most closely matches with the measured pulse amplitude when the spectral phase applied corresponds to a GDD of $+/-12{,}300$ fs^2 and a TOD of $+60{,}000$ fs^3 [Fig. 7]. The sign of the second-order dispersion term in the spectral phase is unknown until additional measurements can determine whether it is positive or negative. A simple way to resolve this ambiguity the is to remeasure the cross-correlation signal after inserting material of known dispersion into the beam path of the idler pulse to be measured. We used a 5-mm-thick sapphire window with dispersion of $-19{,}880$ fs^2 at 5 μm. After inserting this material, the measured cross-correlation signal was compressed to 450 fs [Fig. 6(a)], signifying that the original mid-IR pulse had positive GDD, and the recompressed pulse must have a GDD of -7580 fs^2. This claim was further confirmed by tracing the beam path through the optical setup and estimating the amount of dispersion present by linearly adding the dispersion terms from propagating through each optical element with known dispersion. The amplified 5-μm idler pulse has an estimated GDD of $+12{,}000$ fs^2, mainly due to the contribution from the germanium stretcher after the OPG stage. Recompression to transform-limited pulse duration after amplification can be achieved by adding 3 mm of sapphire to the amplified idler beam path, thereby compensating the dispersion of the pulse to generate pulses containing fewer than 6 optical cycles of the carrier frequency at 5 μm.

7. Conclusion

Advanced technology for production of ultrafast pulses spanning the mid-IR spectral region is needed to exploit the many advantages offered by using longer driving laser wavelengths in areas of IR spectroscopy and strong-field physics. We have developed and characterized a robust design for generating ultrashort mid-IR laser pulses centered at a wavelength of 5 μm in a two-stage OPA based on ZGP crystals that can be pumped directly in the mid-IR to extend the tunability to longer wavelengths. The overall conversion efficiency of the OPA is measured to be approximately 8%. We anticipate that the efficiency could be significantly improved by further optimizing pump conditions on each OPA stage with dispersion management, as suggested by

simulations.

The mid-IR pulses generated in the OPA described contain 26 optical cycles at 5 μm. One approach to generating laser pulses closer to transform-limited duration would be to reduce the amount of CaF_2 and BK-7 encountered by the pulses in the current design. Replacing CaF_2 lenses with off-axis parabolic mirrors or replacing BK-7 dichroic beam combiners with interaction geometries using small non-collinear angles could reduce the total GDD in the system, thereby requiring less material for dispersion compensation and reducing the total TOD. Another approach would be to change the material used for pulse stretching. Germanium has a high refractive index across the mid-IR range (>4), leading to large losses from surface reflections. Germanium also adds significant TOD that cannot be compensated using only materials. Zinc selenide is a viable alternative to germanium due to lower surface reflection losses ($n \approx 2.4$) and less TOD. The material thickness of zinc selenide would need to be 10 times that of germanium, but the use of a right-angle prism pair could provide the longer material lengths needed and would allow for adjustable dispersion compensation. The reduction of TOD on the pulses is particularly useful at longer wavelengths, where the TOD of many materials increases significantly.

Acknowledgments

This research was performed under appointment to the Nuclear Energy University Programs Fellowship sponsored by the U.S. Department of Energy (DOE). Additional support was provided by the Defense Advanced Research Projects Agency (DARPA) under Contract No. N66001-11-1-4197.

#258356 Received 28 Jan 2016; revised 22 Feb 2016; accepted 25 Feb 2016; published 2 Mar 2016